

Optimal Oscillation Damping Control of cable-Suspended Aerial Manipulator with a Single IMU Sensor

Yuri S. Sarkisov^{1,2}, Min Jun Kim¹, Andre Coelho¹,
Dzmitry Tsetserukou², Christian Ott¹, and Konstantin Kondak¹

Abstract—This paper presents a design of oscillation damping control for the cable-Suspended Aerial Manipulator (SAM). The SAM is modeled as a double pendulum, and it can generate a body wrench as a control action. The main challenge is the fact that there is only one onboard IMU sensor which does not provide full information on the system state. To overcome this difficulty, we design a controller motivated by a simplified SAM model. The proposed controller is very simple yet robust to model uncertainties. Moreover, we propose a gain tuning rule by formulating the proposed controller in the form of output feedback linear quadratic regulation problem. Consequently, it is possible to quickly dampen oscillations with minimal energy consumption. The proposed approach is validated through simulations and experiments.

I. INTRODUCTION

Aerial manipulation is a modern and prospective field in interaction robotics with a significant number of industrial applications, especially in remotely located and dangerous environment [1]–[4]. Recently a new branch in this field has begun to emerge: a robotic manipulator is decoupled from the aerial carrier using, for instance, a cable [5], [6]. The main motivation for such an approach includes the ability to operate in a narrow and complex environment.

The main challenge to utilize such systems in real world scenarios is the pendulum motion caused by the cable. It is important to damp out the oscillation as quickly as possible when it occurs due to any disturbances such as the motion of aerial carrier, robotic arm’s motion, or wind gust. To this end, one may control the aerial carrier [7], [8] to cancel out the oscillations. However, these methods can provide only indirect damping for the oscillations.

To damp out the oscillations directly, we can consider to have actuation means on the manipulation platform [9]. We recently developed so-called cable-Suspended Aerial Manipulator (SAM) platform which is equipped with propulsion units to dampen any oscillations, see Fig. 1. Since it is suspended by a cable, the diameter of propellers might be small as its own weight is supported by the aerial carrier; one may refer to [10]–[12] for more details about design and application of the SAM. Therefore, the manipulator can



Fig. 1. The cable-suspended aerial manipulator (SAM) in action.

perform an arbitrary manipulation task while the multi-rotor platform is responsible for the oscillation damping.

However, as will be discussed in detail later, the SAM behaves like a double pendulum, not a single pendulum. Since the motion of a double pendulum is more complex, the onboard IMU sensor does not provide all the states needed for the damping control.

In this paper, to overcome this issue, we design a controller motivated by a simplified model of the SAM. Moreover, we consider two criteria in the control design. First, as addressed earlier, oscillation damping should be accomplished as quickly as possible to perform manipulation tasks. Second, since the aerial system is operated by a battery, we should take the power consumption into account. To this end, we seek an optimal controller that minimizes linear quadratic function that balances two criteria. Through the simulation and experimental validations, the proposed controller turns out to be robust while having a simple form.

The rest of the paper is organized as follows. Section II gives a brief overview of the SAM platform and presents its mathematical model. Section III describes control design, stability analysis, and optimal gain selection strategy. Section IV shows simulation and experimental validation of the designed controller. Finally, section V concludes the paper.

The funding of the European Commission to the AEROARMS project under the H2020 Programme (Grant Agreement 644271) is acknowledged.

¹The authors are with Institute of Robotics and Mechatronics, German Aerospace Center (DLR), Wessling, Germany.

²The authors are with Space CREI, Skolkovo Institute of Science and Technology (Skoltech), Moscow, Russia.

e-mails: iurii.sarkisov@dlr.de,
minjun.kim@dlr.de, andre.coelho@dlr.de,
d.tsetserukou@skoltech.ru, Christian.Ott@dlr.de,
Konstantin.Kondak@dlr.de

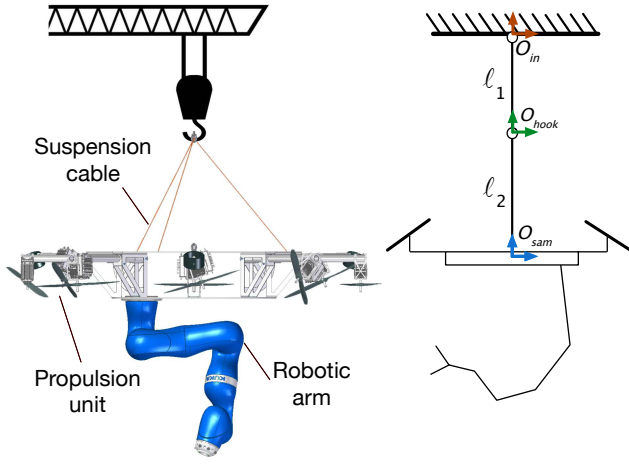


Fig. 2. The SAM platform.

II. THE SAM PLATFORM

In this section, we briefly introduce the SAM platform, including actuation, sensing systems, and mathematical model.

A. System overview

The SAM is an aerial manipulation platform which was designed to perform various manipulation tasks in complex industrial sites. As shown in Fig. 2, the SAM is suspended on the hook of an overhead crane by means of cables¹ and equipped with a robotic arm. In pair with the crane, the SAM can approach most of the task locations. Once it is close to the target, a torque-controlled 7 degrees of freedom (DoF) robotic arm performs a manipulation task. As an example, Fig. 3 shows how SAM is performing mobile crawler deployment on the pipe. In this task, the SAM should press the cage of the crawler at the top of the pipe with certain force to maintain enough contact force. This task is challenging because rather precise positioning should be maintained (to avoid collision) under the environmental contact which may significantly disturb SAM's motion.

To accomplish this task, self-stabilization of the SAM is essential. In particular, this paper is interested in oscillation damping of the SAM, because it is important to dissipate the SAM's motion in order to perform manipulation precisely. To this end, the SAM is equipped with 8 propulsion units with full actuation capability. By properly orienting the propellers, omnidirectional wrench (i.e., 6 DoF torques and forces) can be generated at the geometric center of the SAM platform [13].

The SAM is equipped with various sensors including IMU, 3D-vision camera, and GPS with RTK support. For our controller, we rely only on the IMU sensor, because it is the most robust one among all options. Indeed, GPS may not provide an accurate position in a complex industrial or indoor environment, and the reliability of the vision sensor is limited by the lighting conditions. In contrast, modern

¹Overhead crane can be often found in many industrial spots. Depending on the application, other carriers, e.g., mobile crane or manned/unmanned helicopter, can be exploited with the SAM platform.

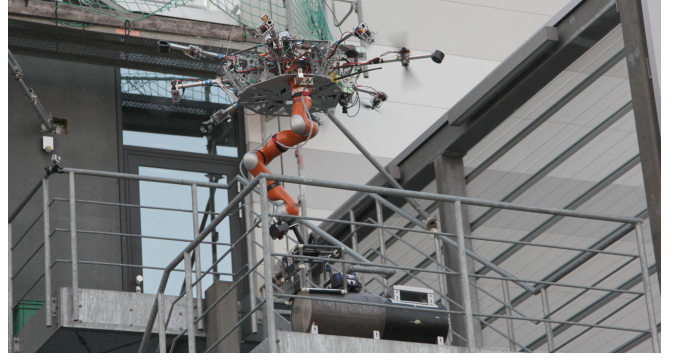


Fig. 3. Crawler deployment on the pipe using the SAM platform.

IMU with AHRS functionalities exploits real-time gyroscope drift correction and yaw adaptation to the disturbed magnetic environment [14].

In this paper, by exploiting the full actuation, we propose an optimal oscillation damping controller of the SAM, using a single onboard IMU sensor.

B. Modeling of the SAM

The SAM suspended on the crane can be modeled as a spherical double pendulum, where the first link is a chain between crane tip and crane hook with length l_1 , and the second link is the distance between hook and platform itself with length l_2 , see Fig. 2. Thus, the state of such a system can be described by 6 variables: the Euler angles of the first ($q_1 \in \mathbb{R}^3$) and the second ($q_2 \in \mathbb{R}^3$) spherical passive joints of the double pendulum.

Let us introduce three coordinate frames. SAM frame (O_{sam}) is located at the center of mass (CoM) of the SAM platform, while its z axis is aligned with the second link and directed upward. Hook frame (O_{hook}) is placed at the second spherical passive joint, and its z axis is aligned with the first link and also directed upward. Finally, O_{in} represents the inertial frame. Initially, its orientation coincides with the SAM frame at the moment when onboard IMU is initialized. Onboard IMU provides orientation and angular velocity w_b of the platform relative to the inertial frame. The weight of the links is neglected, and the two masses, which correspond to the weight of the hook and SAM, are located at the origins of the O_{hook} and O_{sam} frames respectively.

It is worth mentioning that joints of the double pendulum are not actuated, i.e., they are passive. To control the SAM, as described previously, we can apply body wrench $u = [F^T T^T]^T$ at the origin of O_{sam} frame using propulsion units. Based on the preceding description, the equation of motion for the SAM can be written as:

$$M(q)\ddot{q} + C(q, \dot{q})\dot{q} + g(q) = \begin{bmatrix} J^T u \\ \tau_m \end{bmatrix}, \quad (1)$$

where M is the inertia matrix, C is the centrifugal/Coriolis terms, and g is the gravity vector. The configuration q is:

$$q = [q_1^T q_2^T q_m^T]^T. \quad (2)$$

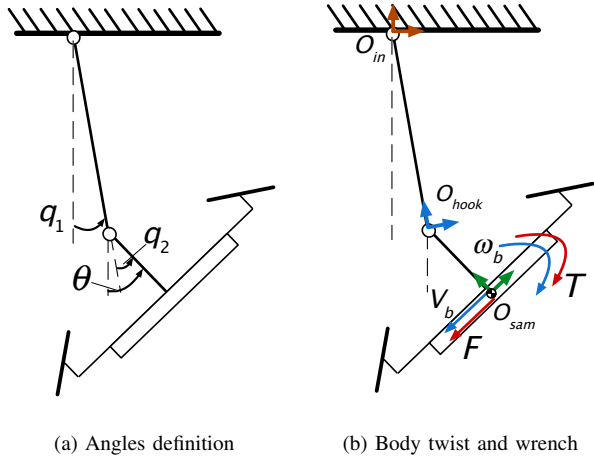


Fig. 4. Planar SAM.

Here, q_m, τ_m represent the generalized coordinates and torque input of the robotic arm. J is the Jacobian matrix that maps $[q_1^T \ q_2^T]^T$ to body twist.

III. OSCILLATION DAMPING CONTROL OF THE SAM

A. Control goal

The equilibrium point (or operating point) of interest corresponds to the bottom position with the stretched configuration of the SAM, i.e., where the potential energy is minimum. Any external perturbation in this position can cause oscillation of the SAM. In fact, due to the presence of the internal joint damping, the system itself is asymptotically stable to the equilibrium point without any control. However, the value of the damping is very low, so natural stabilization takes a long time which is not acceptable for real industrial scenarios. Therefore, our goal is to design an oscillation damping controller to achieve faster damping behavior with minimal power consumption. One challenge is that, as will be shown shortly, the IMU sensor does not provide enough information for the control. To overcome this, in the following section, we restrict the SAM's motion to a plane to get some useful insights.

B. Reduced model for control design

In this paper, we consider a decentralized control approach. Namely, the SAM control and manipulator control are decoupled. Regardless of chosen control strategy [15], [16] and compensators [17], [18] for robotic arm, from SAM's point of view, the dynamic behavior of manipulator is treated as an external disturbance that causes oscillations. Also, experimentally we find out that yaw control of the SAM can be independently performed because (i) we have a good control authority in yaw direction, and (ii) dynamics of yaw is rather decoupled from the others around the operating point. Indeed, we could achieve very strong yaw control by applying a common geometric control approach [19].

Therefore, we can eliminate yaw- and manipulator-related variables in (1), which then reduces to

$$\tilde{M}(\bar{q})\ddot{\bar{q}} + \tilde{C}(\bar{q}, \dot{\bar{q}})\dot{\bar{q}} + \tilde{g}(\bar{q}) = \tilde{J}^T \bar{u} + d, \quad (3)$$

where $\bar{q} = [\bar{q}_1^T \ \bar{q}_2^T]^T$ is a configuration (2) without variables related to yaw and manipulator; \tilde{M} , \tilde{C} , \tilde{g} , and \tilde{J} represent components of remaining dynamics of (1). Motion of manipulator causes an uncertain disturbance d that we further omit and treat as a source of oscillations that have to be dampened by controller.

If we restrict the pendulum motion in the plane (see Fig. 4), we can further simplify the model as follows:

$$\bar{M}(\bar{q})\ddot{\bar{q}} + \bar{C}(\bar{q}, \dot{\bar{q}})\dot{\bar{q}} + \bar{g}(\bar{q}) = \bar{J}^T \bar{u}, \quad (4)$$

where, $\bar{q} = [q_1 \ q_2]^T$ corresponds to angles of first and second links, and $\bar{u} = [F \ T]^T$ is the control wrench, see Fig. 4. The IMU measurement is then $\theta = q_1 + q_2$ for the planar case. The body twist $V = [v_b \ w_b]^T$ and configuration \bar{q} are related by the Jacobian matrix:

$$\underbrace{\begin{pmatrix} v_b \\ w_b \end{pmatrix}}_{=V} = \underbrace{\begin{bmatrix} l_1 \cos q_2 + l_2 & l_2 \\ 1 & 1 \end{bmatrix}}_{=\bar{J}} \underbrace{\begin{pmatrix} \dot{q}_1 \\ \dot{q}_2 \end{pmatrix}}_{=\dot{\bar{q}}}. \quad (5)$$

In a certain range of q_2 ($q_2 < 90^\circ$), the Jacobian matrix \bar{J} is invertible.

In the later section, we design a controller using the simplified planar model, while stability analysis is performed for the original system model (3).

C. Behavior of planar double pendulum

For later convenience, we present some insights on the behavior of planar double pendulum. Basically, any double pendulum system contains two oscillation motions [20]: the first component with low frequency, ν_{slow} , is modulating the second one with high frequency, ν_{fast} . Although the solution for joint angles q_1 and q_2 contains both high and low frequency motions, in the system with parameter relation such as $l_1 > l_2$ and $m_1 < m_2$, roughly speaking, q_1 is dominated by slow motion and q_2 by fast motion.

Fast and slow frequencies of the planar double pendulum system can be calculated using the following:

$$\nu_{fast,slow}^2 = \frac{gm_{12}}{8\pi^2 m_1 l_1 l_2} \left((l_{12}) \pm \sqrt{l_{12}^2 - \frac{4m_1 l_1 l_2}{m_{12}}} \right). \quad (6)$$

Here, m_1 is a weight of the hook, m_2 is the weight of the platform, $m_{12} = m_1 + m_2$, and $l_{12} = l_1 + l_2$.

D. Control design

In the planar model in (4), we first apply coordinate transformation from \bar{q} to V using (5). Then, we obtain

$$\Lambda(\bar{q})\dot{V} + \Gamma(\bar{q}, \dot{\bar{q}})V + \zeta(\bar{q}) = \bar{u}, \quad (7)$$

where Λ, Γ, ζ represent inertia, Coriolis/centrifugal, gravity in the new coordinate system. This coordinate transformation is valid since the Jacobian matrix \bar{J} is invertible. From (7), damping can be artificially injected by simply letting

$$\bar{u}_{des} = \begin{bmatrix} F \\ T \end{bmatrix} = \begin{bmatrix} -K_v v_b \\ -K_w w_b \end{bmatrix}, \quad (8)$$

where K_v, K_w are positive control gains. Using (8), the control goal addressed earlier can be achieved.

However, this control law cannot be directly applied because we have no measurements for v_b , whereas w_b is directly obtained by IMU sensor. Assuming small angle for q_2 (hence $\cos(q_2) \simeq 1$), from (5), F can be approximated as

$$F = -K_v(l_1\dot{q}_1 + l_2w_b). \quad (9)$$

As addressed in Section III-C, \dot{q}_1 is dominated by slow oscillation motion with a low-frequency mode while w_b contains both modes. Therefore, we can extract \dot{q}_1 from $w_b = \dot{\theta}$ by taking low-pass filter, and then (8) can be rewritten as

$$\bar{u} = \begin{bmatrix} F \\ T \end{bmatrix} = \begin{bmatrix} -K_v(l_1w_b^{lp} + l_2w_b) \\ -K_w w_b \end{bmatrix}, \quad (10)$$

where

$$w_b^{lp} = \frac{1}{\tau s + 1} w_b \quad (11)$$

is the low-pass filter with the time constant τ .

We extend the presented control law to the original system (3) as follows

$$\bar{u} = \begin{bmatrix} F \\ T \end{bmatrix} = \begin{bmatrix} -K_v(l_1w_b^{lp} + l_2w_b) \\ -K_w w_b \end{bmatrix} \quad (12)$$

In our control design, the cut-off frequency of the low-pass filter is selected in the middle between slow and high frequency modes, i.e.,

$$\nu_{cutoff} = \frac{\nu_{slow} + \nu_{fast}}{2}. \quad (13)$$

E. Closed-loop stability

Since the double pendulum system with damping in joints is asymptotically stable by nature, we investigated the stability of our controller in a simulator. We report that for the $l_1 = 4..10[m]$ while changing the initial angles of the passive joints from 2 till 45 degrees in arbitrary configuration with a step of 7 degrees, the closed-loop system was always stable. Moreover, initial angular velocities at these joints were varied from 0 to 1 $\frac{rad}{s}$ with a step of 0.5. Performed analysis also confirms that the proposed controller is robust against model uncertainties.

F. Gain tuning rule

Since the system is stable for (almost) any choice of parameters and gains, it is important to seek the best gain in some sense. In particular, we seek for the control gains which minimize the following linear quadratic cost function

$$J = \int_0^t (X(t)^T Q X(t) + U(t)^T R U(t)) dt, \quad (14)$$

where $Q \geq 0$ penalizes the state X , and $R > 0$ penalizes the amount of control input U .

In this subsection, we again use the planar double pendulum for simplicity. Also, we use $\dot{\theta}$ (which is equivalent to w_b in planar case) for the body angular velocity in this subsection just to have a nicer look. Let us first linearize (4) around operating point as follows

$$\dot{X} = AX + BU, \quad (15)$$

where $X = [q_1 \ \dot{q}_1 \ \theta \ \dot{\theta}]^T$, with

$$A = \begin{pmatrix} 0 & 1 & 0 & 0 & 0 \\ -\frac{gm_{12}}{m_1 l_1} & 0 & \frac{m_2 g}{m_1 l_1} & 0 & 0 \\ 0 & 0 & 0 & 1 & 0 \\ \frac{gm_{12}}{m_1 l_2} & 0 & -\frac{gm_{12}}{m_1 l_2} & 0 & 0 \\ 0 & 0 & 0 & \frac{1}{\tau} & -\frac{1}{\tau} \end{pmatrix}, \quad (16)$$

$$B = \begin{pmatrix} 0 & 0 \\ 0 & -\frac{1}{m_1 l_1 l_2} \\ 0 & 0 \\ \frac{1}{m_2 l_2} & \frac{m_{12}}{m_1 m_2 l_2^2} \\ 0 & 0 \end{pmatrix}. \quad (17)$$

The last row of matrix A corresponds to the dynamics of the low-pass filter:

$$\tau \ddot{\theta}^{lp} + \dot{\theta}^{lp} = \dot{\theta}. \quad (18)$$

To make the control input (10) have output feedback form, we define output as

$$Y = CX, \quad (19)$$

where

$$C = \begin{pmatrix} 0 & 0 & 0 & l_2 & l_1 \\ 0 & 0 & 0 & 1 & 0 \end{pmatrix}. \quad (20)$$

Consequently, the control input U is expressed as the output feedback form:

$$U = -FY = - \begin{bmatrix} K_v & 0 \\ 0 & K_w \end{bmatrix} Y. \quad (21)$$

For our system described by (15)-(19), we applied the output feedback LQR technique which can be formulated using linear matrix inequalities (LMIs).

Theorem 1: Let us consider the system (15) with the output (19). There exists an optimal controller in the form of (21) which minimizes the cost function (14), if the following problem has a solution for the given matrix $\Xi > 0$ and weighting matrices $Q \leq 0$, $R > 0$:

$$\min_{F, P} \text{trace}(P), \quad (22)$$

subject to LMIs:

$$M \leq 0, \quad P > 0,$$

where

$$M = \begin{bmatrix} A^T P + P A + Q + H & G^T \\ G & -R^{-1} \end{bmatrix}, \quad (23)$$

with

$$G = FC - R^{-1} B^T P, \quad (24)$$

$$H = -(\Xi B) R^{-1} (B^T P) - (PB) R^{-1} (B^T \Xi) + (\Xi B) R^{-1} (B^T \Xi). \quad (25)$$

To solve the given LMI problem, we used `oflqr` library [21] with the LMI solver in YALMIP [22]. In our control design, we selected Q and R matrices as follows:

$$Q = \text{diag}\{0, 10, 0, 1, 0\} \text{ and } R = \sigma \cdot \text{diag}\{1, 10\}. \quad (26)$$

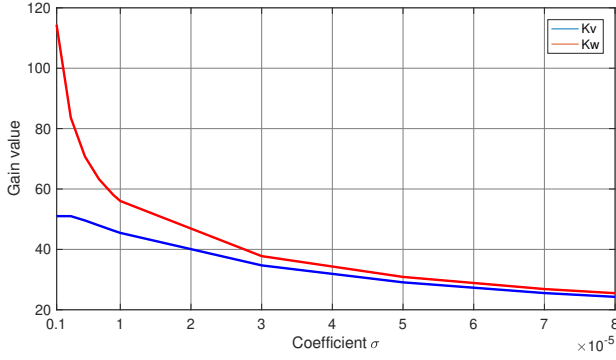


Fig. 5. Relation between optimal control gains K_v, K_w and parameter σ .

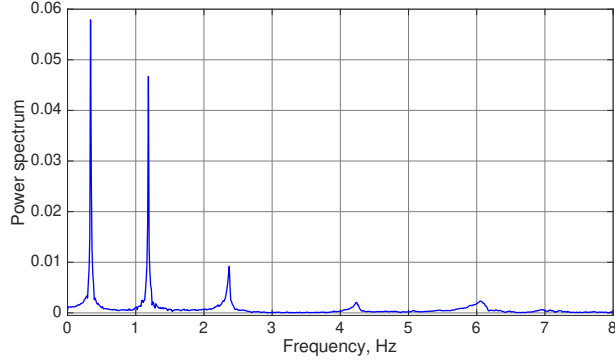


Fig. 6. Power spectrum of real system.

Since our control goal is to dampen the oscillations, we penalized only \dot{q}_1 and $\dot{\theta}$. Moreover, we applied stronger control action on slow oscillation mode which might be more critical when performing manipulation tasks in a real industrial scenario. For this reason, we penalized \dot{q}_1 more than $\dot{\theta}$ in \mathbf{Q} , and allowed more control input for F in \mathbf{R} design.

In (26), σ is a new parameter that allows us to investigate optimal control gains over admissible control inputs; note that smaller \mathbf{R} implies larger control input. Therefore, we solved the optimization problems with varying σ : from $1e^{-6}$ to $8e^{-5}$, as shown in Fig. 5. Depending on the designer's choice (balance between oscillation damping and power consumption), we can select one good combination of gains.

Optimization was conducted using parameters measured in the real system:

$$m_1 = 18.5 [kg], \quad m_2 = 55 [kg], \quad l_1 = 6 [m], \quad l_2 = 2.2 [m] \quad (27)$$

As a time constant for low-pass filter, cut-off frequency $\nu_{cutoff} = 0.76 [Hz]$ was calculated based on (13). Oscillation mode frequencies ν_{slow} and ν_{fast} were obtained from the real hardware, as shown in Fig. 6.

IV. VALIDATION

In order to validate the proposed controller, numerical simulation and experiments were conducted. For both cases, to control the robotic arm and to perform oscillation damp-

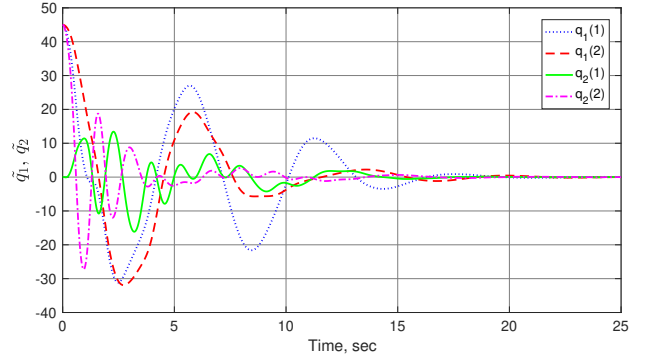


Fig. 7. State convergence with extreme initial conditions.

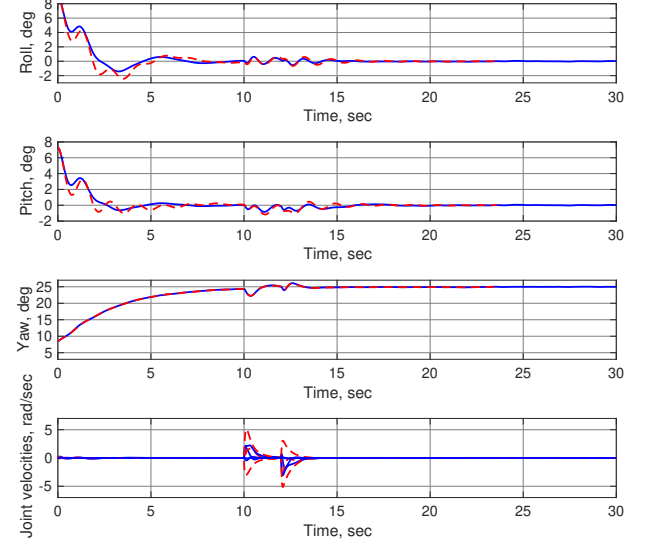


Fig. 8. Comparison of the proposed (blue) and ideal (red) controllers.

ing while keeping constant yaw, the decentralized control approach was applied as we addressed in Section III-B.

A. Validation of double pendulum model

To see the validity of the double pendulum model, we investigated oscillation modes of the real hardware during the free motion. To this end, we lifted up the SAM and then released. We applied fast Fourier transform to obtain a power spectrum. As shown in Fig. 6, there exist two dominant frequency modes, and therefore, it is reasonable to model the system as a double pendulum.

B. Numerical simulations

Numerical simulation was conducted based on [23] which proposed an algorithm that computes dynamic parameters efficiently. The SAM platform was modeled as a spherical double pendulum. In this simulation, all parameters were chosen to be as close as possible to the real setup. To this end, in addition to the model parameters given in (27), gyro noise density $0.009 [^\circ/s/\sqrt{Hz}]$ was taken from calibration certificate provided by the manufacturer of IMU. However, influence of unmodeled dynamics (e.g., weight of the link), airflow, and actuator dynamics is not considered in

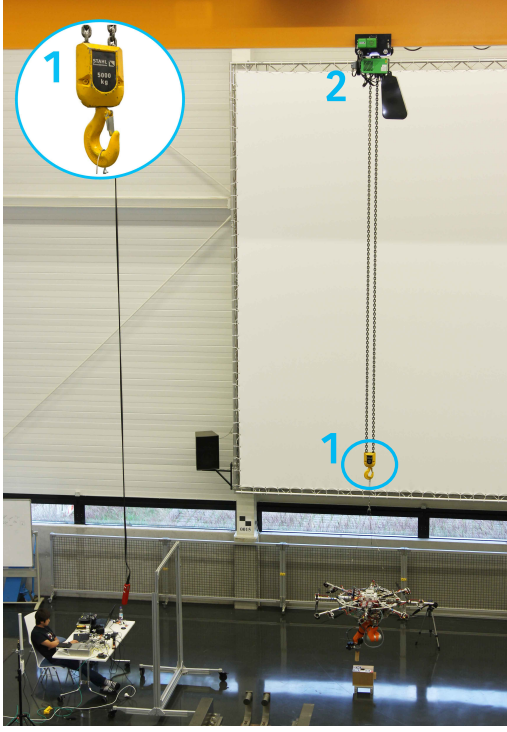


Fig. 9. Experimental setup: 1 is hook, 2 is winch.

the simulation. Performance under all uncertainties will be validated through experiments.

In this subsection, we present two simulation studies. First, we validate stability of the proposed controller. As addressed in Section III-E, we investigated stability for large variations of initial conditions including those which are far from normal operating range. In our experience, the SAM was never excited more than 5° for roll/pitch. Nevertheless, we set 45° for all initial angle values as an extreme case. As shown in Fig. 7, all system states converged to the equilibrium point, which indicates asymptotic stability.

Second, we compare the proposed control law (12), and the ideal controller

$$\mathbf{u}_{des} = \begin{bmatrix} \mathbf{F} \\ \mathbf{T} \end{bmatrix} = \begin{bmatrix} -K_v \mathbf{v}_b \\ -K_w \mathbf{w}_b \end{bmatrix}, \quad (28)$$

which is the 3D version of (8). Recall that we proposed (12) because \mathbf{v}_b is not measurable for the real system. As shown in Fig. 8, overall shapes of resulting behavior were quite similar for both controllers. Actually, the proposed controller resulted in less oscillations compared to the ideal one due to effect of filters. At $t = 10$, the robotic arm was commanded to cause jerky motions to apply some disturbances on the SAM. The simulation validates that the proposed control could dissipate the oscillation caused by the disturbances.

C. Experimental validation

To corroborate simulation results, experimental validation was carried out using the overhead crane. Our experimental setup is shown in Fig. 9. Blue digits mark the elements (winch and hook) which correspond to the two passive spherical joints. Hook has a passive DoF around the yaw,

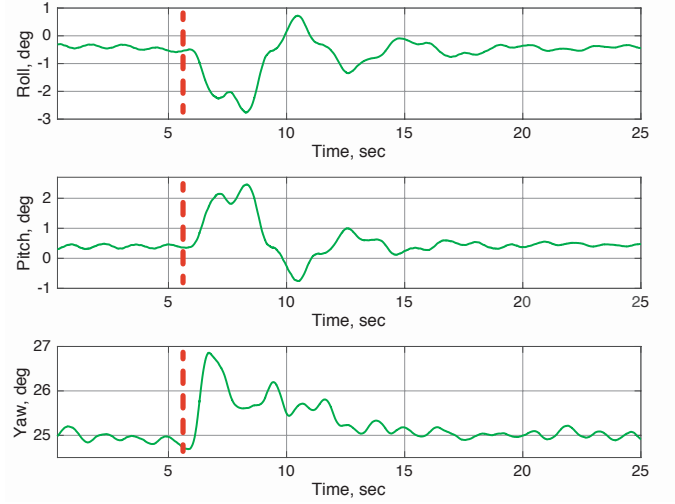


Fig. 10. Experimental results. Red dashed line marks the time at which external disturbances were applied to the system.

i.e., hook itself can rotate around the hook base. The chain of the winch can twist around a vertical axis.

The selected optimal control gains were $K_v = 48$, $K_w = 70$ with $\sigma = 5e^{-6}$. In the experiment, human applied external disturbance to excite the SAM, while the controller was trying to dampen any oscillations. As shown in Fig. 10, the controller quickly damped out the oscillation within 6 seconds. Please see also the video attachment in which we have compared the convergence rate of the passive system and controlled system under the effect of different disturbances, e.g., external perturbations, moving suspension point, and jerky motion of the robotic arm.

V. SUMMARY AND CONCLUDING REMARKS

In this paper, the oscillation damping control approach for the SAM platform was designed, applied, and validated in simulation and experimental studies. The system in operation can be considered as a spherical double pendulum, which can be controlled only indirectly by generating a damping wrench at the tip of the second link. Due to the absence of the state measurements, damping wrench was generated by proposed controller using only onboard IMU without any model parameters. Additionally, we found the optimal control gains which minimize the linear quadratic cost function, so the resulting controller dissipates the oscillation with desired balance between performance and power consumption. Moreover, by virtue of the optimal gains, we can easily tune the gains for different operating conditions.

Although local stability could be shown theoretically, we presented some evidence from which stability in reasonably large operating range could be expected. Performance of the controller can be further improved by considering the motion of the robotic arm as a part of the system and by fusing additional sensor information, e.g., GPS RTK or 3D-vision. In the future, we plan to design a controller that adapts to varying link length (which is controllable by the crane) and battery status (for instance, more weights on the control input when the battery is low).

REFERENCES

- [1] F. Ruggiero, V. Lippiello, and A. Ollero, "Aerial manipulation: A literature review," *Robotics and Automation Letters*, vol. 3, no. 3, pp. 1957–1964, 2018.
- [2] H. B. Khamseh, F. Janabi-Sharifi, and A. Abdessameud, "Aerial manipulation—a literature survey," *Robotics and Autonomous Systems*, vol. 107, pp. 221–235, 2018.
- [3] A. Ollero, G. Heredia, A. Franchi, G. Antonelli, K. Kondak, A. S. Cortes, A. Viguria, J. R. Martinez-de Dios, F. Pierri, J. Cortes *et al.*, "The aeroarms project: Aerial robots with advanced manipulation capabilities for inspection and maintenance," *IEEE Robotics & Automation Magazine*, no. 99, pp. 1–1, 2018.
- [4] M. J. Kim, K. Kondak, and C. Ott, "A stabilizing controller for regulation of uav with manipulator," *Robotics and Automation Letters*, vol. 3, no. 3, pp. 1719–1726, 2018.
- [5] A. Suárez, P. Sanchez-Cuevas, M. Fernandez, M. Perez, G. Heredia, and A. Ollero, "Lightweight and compliant long reach aerial manipulator for inspection operations," in *IEEE/RSJ International Conference on Intelligent Robots and Systems (IROS)*, 2018, pp. 6746–6752.
- [6] R. Miyazaki, R. Jiang, H. Paul, Y. Huang, and K. Shimonomura, "Long-reach aerial manipulation employing wire-suspended hand with swing-suppression device," *IEEE Robotics and Automation Letters*, vol. 4, no. 3, pp. 3045–3052, 2019.
- [7] B.-Y. Lee, H.-I. Lee, D.-W. Yoo, G.-H. Moon, D.-Y. Lee, Y. young Kim, and M.-J. Tahk, "Study on payload stabilization method with the slung-load transportation system using a quad-rotor," in *European Control Conference (ECC)*. IEEE, 2015, pp. 2097–2102.
- [8] M. Yoshikawa, A. Iwatani, and J. Ishikawa, "Damping control of suspended load for truck cranes in consideration of control input dimension," in *International Conference on Advanced Engineering Theory and Applications*. Springer, 2017, pp. 436–446.
- [9] M. J. Kim, J. Lin, K. Kondak, D. Lee, and C. Ott, "Oscillation damping control of pendulum-like manipulation platform using moving masses," *IFAC-PapersOnLine*, vol. 51, no. 22, pp. 465–470, 2018.
- [10] Y. S. Sarkisov, M. J. Kim, D. Bicego, D. Tsetserukou, C. Ott, A. Franchi, and K. Kondak, "Development of sam: Cable-suspended aerial manipulator," in *International Conference on Robotics and Automation (ICRA)*. IEEE, 2019, pp. 5323–5329.
- [11] J. Lee, R. Balachandran, Y. S. Sarkisov, M. De Stefano, A. Coelho, K. Shinde, M. J. Kim, R. Triebel, and K. Kondak, "Visual-inertial telepresence for aerial manipulation," in *IEEE International Conference on Robotics and Automation (ICRA)*, 2020, accepted.
- [12] A. Coelho, H. Singh, C. Ott, and K. Kondak, "Whole-body bilateral teleoperation of a redundant aerial manipulator," in *IEEE International Conference on Robotics and Automation (ICRA)*, 2020, accepted, available online: <http://arxiv.org/abs/2001.10779>.
- [13] A. Franchi, R. Carli, D. Bicego, and M. Ryll, "Full-pose tracking control for aerial robotic systems with laterally bounded input force," *Transactions on Robotics*, vol. 34, no. 2, pp. 534–541, 2018.
- [14] "Mti 100-series description," [accessed 5-September-2019]. [Online]. Available: <https://www.xsens.com/products/mti-100-series/>
- [15] A. Albu-Schäffer, C. Ott, and G. Hirzinger, "A unified passivity-based control framework for position, torque and impedance control of flexible joint robots," *The international journal of robotics research*, vol. 26, no. 1, pp. 23–39, 2007.
- [16] D. Tsetserukou, N. Kawakami, and S. Tachi, "Vibration damping control of robot arm intended for service application in human environment," in *8th IEEE-RAS International Conference on Humanoid Robots*. IEEE, 2008, pp. 441–446.
- [17] M. Iskandar and S. Wolf, "Dynamic friction model with thermal and load dependency: modeling, compensation, and external force estimation," in *International Conference on Robotics and Automation (ICRA)*. IEEE, 2019, pp. 7367–7373.
- [18] M. J. Kim, F. Beck, C. Ott, and A. Albu-Schäffer, "Model-free friction observers for flexible joint robots with torque measurements," *IEEE Transactions on Robotics*, vol. 35, no. 6, pp. 1508–1515, 2019.
- [19] T. Lee, M. Leok, and N. H. McClamroch, "Geometric tracking control of a quadrotor uav on se (3)," in *49th IEEE conference on decision and control (CDC)*, 2010, pp. 5420–5425.
- [20] K. Magnus, *Vibrations*. Blackie & Son, 1965.
- [21] A. Ilka, "Matlab/octave toolbox for structurable and robust output-feedback lqr design," *IFAC-PapersOnLine*, vol. 51, no. 4, pp. 598–603, 2018.
- [22] J. Löfberg, "Yalmip: A toolbox for modeling and optimization in matlab," in *Proceedings of the CACSD Conference*, vol. 3. Taipei, Taiwan, 2004.
- [23] G. Garofalo, C. Ott, and A. Albu-Schäffer, "On the closed form computation of the dynamic matrices and their differentiations," in *IEEE/RSJ International Conference on Intelligent Robots and Systems (IROS)*, 2013, pp. 2364–2359.